PCCP

Accepted Manuscript

ROYAL SOCIETY OF CHEMISTRY

www.rsc.org/pccp

Table of contents entry

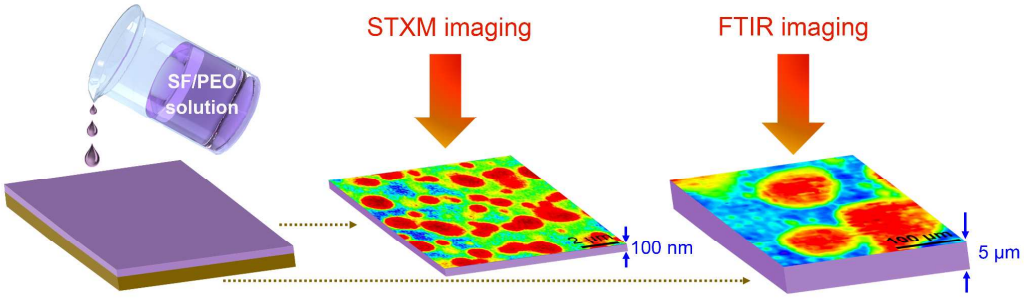

The combination of FTIR and STXM imaging provides complimentary information that enable greater understanding of protein-based polymer blend. Both techniques can monitor the phase separation behavior of SF/PEO blends, but more importantly, FTIR imaging can tell the conformation difference while STXM imaging can provide composition of two components in two phases.

Cite this: DOI: 10.1039/c0xx00000x

www.rsc.org/xxxxxx

PAPER

Structural determination of protein-based polymer blends with a promising tool — Combination of FTIR and STXM spectroscopic imaging

Shengjie Ling,[a] Zeming Qi,[b] Benjamin Watts,[c] Zhengzhong Shao[a] and Xin Chen*[a]

Received (in XXX, XXX) Xth XXXXXXXXX 20XX, Accepted Xth XXXXXXXXX 20XX
DOI: 10.1039/b000000x

Fourier transform infrared (FTIR) and scanning transmission X-ray microscopy (STXM) spectroscopic imaging techniques are introduced to determine the structure of protein-based polymer blends, using silk fibroin/polyethylene oxide (SF/PEO) blend as a model material. We demonstrate that FTIR and STXM imaging provide complimentary chemical sensitivities, resolution ranges and sample thickness requirements that can enable greater understanding of SF/PEO blend films. From the FTIR images, we find SF shows random coil and/or helical conformation in the SF-rich domains, and β-sheet conformation in the PEO-rich matrix. In the meantime, the SF content in SF-rich domains is 74±4%, and 38±6% in PEO-rich matrix from the STXM images. These findings support and give further evidence to the conclusions of the previous studies on SF/PEO blends in the literature. Our results strongly suggest that FTIR and STXM imaging techniques are two promising complementary approaches for the study of phase behaviour and molecular conformation in protein-based polymer blend materials.

Introduction

Silk fibroin (SF) is a widely used and studied protein polymer for a variety of task-specific applications.[1,2] In particular, it has recently gained much attention as a biomaterial because of several desirable properties such as biocompatibility and low immunogenicity.[3-5] In order to improve or adapt the properties of silk materials, SF is sometimes blended with other natural or synthetic polymers.[1] As in other polymer blends, the phase behaviour of these SF-based polymer blends is thought to be very important towards their related properties.

Conventional methods used to study phase behaviour in SF-based polymer blends include scanning electron microscopy (SEM),[6-10] atomic force microscopy (AFM),[8,9] differential scanning calorimetry (DSC),[6,11] and dynamic thermomechanical analysis (DTMA).[7,12] Although these analytical methods have provided a great deal of useful information about the phase behaviour of SF-based blends, they cannot directly provide data on chemical structure information within these blends.

Fourier transform infrared (FTIR) imaging, coupled with a step-scan interferometer with an FTIR spectrometer and a focal plane array (FPA) detector, can collect spatial and spectral information of samples simultaneously,[13] thus enabling a real-space chemical visualization of polymer blends. The chemical contrast of FTIR originates from the interaction of infrared light with vibrations within molecules, whose frequencies can be traced to specific motions of particular chemical moieties. Therefore, features in the infrared spectrum associated with an area in an FTIR image indicates the presence of a material, with the conformation of the material affecting the broadening and relative intensity of the absorption bands in characteristic ways. Therefore, FTIR imaging has been used for studying the phase behaviour of polymer blends,[14-16] polymer dissolution processes,[13,17] and the structure changes of polymers under tensile deformation.[16,18] In previous work, we have successfully adopted this technique to study the compatibility of silk fibroin/chitosan (SF/CS), silk fibroin/sodium alginate (SF/SA), and silk fibroin/polyvinyl alcohol (SF/PVA) blends.[19] The results demonstrated that FTIR images of these SF-based blends can provide additional useful information on the composition of each components and the conformations of SF at defined locations. However, a drawback of FTIR imaging is its practical spatial resolution is limited to about 4 × 4 μm. Although a recent report asserts to obtain a high-quality image with a diffraction-limited resolution of 0.54 μm within 30 min by using multiple synchrotron beam FTIR imaging with wide-field FPA detectors,[20] such a technique is still in its infancy and not easy to access.

An alternative approach to image the domain structure in polymer blends is the scanning transmission X-ray microscopy (STXM) technique. Combining the chemical sensitivity of near-edge X-ray absorption fine structure (NEXAFS) with a spot size of 30 nm or less, STXM is a powerful technique that allows for the quantitative determination of polymer blend composition in submicrometer scale.[21-23] The X-ray absorption of sample films are measured in transmission and rastered with respect to the incident beam to produce X-ray absorption images. Used in conjunction with a synchrotron beamline fitted with a high–resolution

monochromator, the probing X-ray beam can be tuned to near-edge resonances and utilize specific spectroscopic effects for tailored image contrast. Thus, STXM imaging at the carbon K-edge (photon energy of approximately 290 eV or conversely a wavelength of about 4.3 nm) provides strong chemical sensitivity and selectivity in organic materials via differences in X-ray absorption spectra that derive from differences in antibonding electronic structure. By combining X-ray absorption images taken at more than two X-ray energies (at which there is a difference in the X-ray absorption of the two materials) with the knowledge of the NEXAFS spectra of pristine component films, it is possible to produce quantitative compositional maps of the blend films.[21,22] While STXM is also sensitive to molecular conformation via linear dichroism,[23] and indeed has been used to investigate silk fibers,[24,25] it is more difficult to observe than in FTIR as it requires certain kinds of asymmetry in both molecular structure and ordering.

Generally speaking, FTIR imaging is more sensitive to protein conformation but with lower spatial resolution and greater tolerance of thicker sample films, while on the other hand, STXM imaging has higher resolution, more quantifiable composition mapping and better tolerance for thinner sample films. Therefore, we believe the integrated use of these two complementary techniques would be a powerful tool for deepening the understanding of the phase behaviour of protein-based polymer blends. In this communication, we choose a SF/PEO blend as an example to study, as it is a promising biomaterial. The bulk and surface features of SF/PEO blends are very useful as bioactive interfaces to stimulate desired cellular responses.[9,10] Furthermore, PEO can be leached from the SF/PEO film to generate defined SF porous structures or microspheres. These porous structures may be utilized to enhance nutrient diffusion, provide filtration, or improve cellular communication through the silk film matrix,[10,26] and the microspheres provide new options for drug delivery due to their tunable drug loading and release properties.[5,26]

Experimental section

Raw *Bombyx mori* (*B. mori*) silk cocoons from Jiangsu Province, China were degummed twice with 0.5% (w/w) $NaHCO_3$ solution at 100°C for 30 min and then washed with distilled water and allowed to air dry at room temperature. The degummed *B. mori* silk fibres were then dissolved in 9.3 mol/L LiBr aqueous solution. After dialysis against deionized water for 3 days at room temperature, the solution was filtered and the resulting SF solution diluted to 1% (w/w) with deionized water. PEO (M_w=900,000) from Sigma-Aldrich was directly dissolved in deionized water without further purification to prepare a 1% (w/w) PEO solution.

The 1% SF solution was gently mixed with 1% PEO solution to give homogeneous solution with the final SF/PEO mass ratio of 80/20. The SF/PEO blend films for FTIR imaging were prepared by casting such a mixture solution onto a polyethylene plate, and allowed to dry at approximately 25°C and 50% relative humidity to give films of an approximate thickness of 5 μm. The SF/PEO blend films for STXM imaging were prepared by casing a drop of the same solution on a highly doped silicon wafer with a final thickness of about 100 nm.

Conventional FTIR spectra were recorded using a Nicolet Nexus 6700 FTIR spectrometer. To eliminate spectral contributions due to atmospheric water vapour, the instrument was continuously purged by dry nitrogen. For each measurement, 256 interferograms were coadded and transformed employing a Genzel-Happ apodization function to yield spectra with a nominal resolution of 4 cm^{-1}.

FTIR imaging was performed using a Bruker imaging system at Beamline U4 in the National Synchrotron Radiation Laboratory (NSRL, Hefei, China), which consists of an IFS66/S step-scan/rapid-scan FTIR spectrometer, a Hyperion 3000 infrared microscope with 15× objective coupled with a 64 × 64 mercury cadmium telluride (MCT) focal plane array (FPA) detector. The samples were imaged in transmission with an individual pixel size of about 4 × 4 μm over a 260 × 260 μm field of view. The FTIR imaging spectra were collected in the mid-infrared (MIR) range of 800–3800 cm^{-1} at a resolution of 4 cm^{-1} with 256 coadded scans. The corresponding collection time for one experiment is about 10 min. All the data collection and processing were performed using OPUS 6.5 (Bruker).

Deconvolution of the amide I bands was carried out using PeakFit 4.12. The number and positions of peaks were defined from the results of the second derivatives of the spectra and fixed during the deconvolution process. As in our previous studies, a Gaussian model was selected for the band shape and the band width was automatically adjusted by the software.[27] Cluster analysis of normalized amide I bands were processed though *k*-means clustering methods with 2 clusters by using Unscrambler v 9.7 (CAMO).

The STXM imaging was performed at PolLux beamline at Swiss Light Source (Paul Scherrer Institute, Villigen, Switzerland).[28-30] Detailed discussion of the STXM technique and its application to organic materials can be found in our previous publication.[31] Briefly, a Fresnel zone plate focuses a monochromatic X-ray beam onto a small spot (typically less than 30 nm) on a thin, semi-transparent sample film, with the transmitted beam intensity being measured by a photo-multiplier tube (PMT; after conversion of the X-rays to visible photons by a phosphor screen) and this value recorded in one pixel position of an array. Raster-scanning the sample, while recording further measurements of the transmitted X-ray beam intensity, fill out the array of pixel-values to produce an image of the sample. STXM measurements presented here were performed with a zone plate with 25 nm outer-most zone width and images for composition mapping were recorded at 280 eV, 288.25 eV, 289.05 eV and 320 eV. The corresponding recording time for one experiment is about 1 h. Data analysis was performed using the aXis2000 software package. [32]

Results and discussion

FTIR images of SF/PEO blend films

In order to distinguish the characteristic absorption bands among SF and PEO, we recorded the high quality conventional FTIR spectra under well-controlled conditions in the same manner as for our previous FTIR imaging studies for SF/CS, SF/GA, and SF/PVA blends.[19] Fig. 1a shows (from bottom to top) the FTIR spectra of SF film as cast, SF film treated with 70% ethanol aqueous solution, pristine PEO film, and SF/PEO blend film. The most important band regions of SF are amide I (1700-1600 cm^{-1}) and amide II (1600-1500 cm^{-1}) because all of these amide

vibrations directly depend on the secondary structure of the protein backbone. The amide I region mainly comes from the C=O stretching vibration (80%) with minor contributions from the N-H in-plane bending.[33] The amide II region is caused mostly by the C-N stretching and the N-H in-plane bending vibration of the backbone.[33] The as-cast SF film (Fig. 1a) shows absorption bands at 1660 cm^{-1} (amide I) and 1540 cm^{-1} (amide II), which are assigned to random coil and/or helical conformation.[27,34-36] After the treatment with 70% ethanol solution, the SF film however shows absorption at 1700 cm^{-1}, 1630 cm^{-1} and 1530 cm^{-1}. The peaks at 1630 cm^{-1} and 1530 cm^{-1} are attributed to β-sheet,[27,34-36] and the shoulder peak at 1700 cm^{-1} is assigned to β-turn conformation associated with the anti-parallel β-sheet structure.[36] In the meantime, the pristine PEO film shows mainly absorption bands at 2887 cm^{-1} (CH_2 stretching) and 1113 cm^{-1} (CO stretching).[37-39] We are happy to see that PEO has no absorption in the 1500 –1700 cm^{-1} region (amide I and amide II bands of SF), so both amide I and amide II bands can be used to analyse the conformational information of SF in the SF/PEO blend. For convenience, the assignments of the major bands of SF and PEO in the FTIR spectra are summarized in Table 1.

Table 1. The FTIR band assignments of SF and PEO*

wavenumbers (cm^{-1})		assignments	reference
SF	1700	amide I, C=O *s*, CN *s*; β-turn	27,33,36
	1660	amide I, C=O *s*, CN *s*; random coil and/or α-helical	27,33-36
	1630	amide I, C=O *s*, CN *s*; β-sheet	27,33-36
	1540	amide II, NH *ib*, CN *s*; random coil and/or α-helical	27,33-36
	1530	amide II, NH *ib*, CN *s*; β-sheet	27,33-36
PEO	2887	CH_2 *s*	37-39
	1469	CH_2 *s*	37-39
	1342	CH_2 *w*	37-39
	1280	CH_2 *t*	37-39
	1242	CH_2 *t*	37-39
	1148	CO *s*	37-39
	1113	CO *s*	37-39
	1103	CO *s*	37-39
	1062	CO *s*, CH_2 *r*, CC *s*	37-39
	963	CH_2 *r*, CH_2 *s*	37-39
	843	CH_2 *r*, CO *s*	37-39

* Abbreviations: *s*= stretching, *ib*= in-plane bending, *w*= wagging, *t*= twisting, *r*= rocking.

In this article, we selected a SF/PEO blend with the mass ratio of 80/20 to investigate, as the phase separation under this ratio was found to be most obvious from both our screening test and the literature.[9] It can be found that SF/PEO blend shows a strong absorption peak at 1630 cm^{-1} (Fig. 1a), indicating PEO induces a conformation transition of SF from random coil to β-sheet similarly as chitosan and sodium alginate.[40,41]

Before the imaging experiment, the non-overlapping bands for SF and PEO should be identified. In this study, we chose amide II of SF (1500-1600 cm^{-1}) and CO stretching band of PEO (1000-1184 cm^{-1}) as SF-specific and PEO-specific absorption, and integrated them for all pixel spectra to obtain chemical images of each component. Meanwhile, in order to reduce the effect on the images caused by variations in thickness across the field of view, inevitable in cast films, the ratios of absorbance of A_{SF}/A_{PEO} (using A_{1540}/A_{1113}) were also integrated. Fig. 1b-d show the resulting FTIR maps of SF absorbance (b), PEO absorbance (c) and their ratios (A_{SF}/A_{PEO}; d), in which red represents the largest integrated intensity and purple (or blue) the weakest integrated intensity in a given field of view for the specific component.

In the SF-specific FTIR image (Fig. 1b), there are "islands" (red) with the size of 80–100 μm embedded in the "sea" (blue). The shape of these red "islands" in SF-specific FTIR image is found to be remarkable complementarity with the blue "islands" in the PEO-specific FTIR image (Fig. 1c). Furthermore, the A_{SF}/A_{PEO} image shows the same pattern (Fig. 1d) as the SF and PEO-specific images, thus it is no doubt that the "islands" is SF-rich phase and the "sea" the PEO-rich phase in SF/PEO blend. In other words, the images in Fig. 1b-d clearly show that the sample is composed of SF-rich enclosed domains and a continuous PEO-rich matrix. The phase separation behaviour of SF and PEO in their blend observed by FTIR imaging in this study is similar to that reported by Kaplan *et al.* with the same SF/PEO ratio.[9] However, the size of SF phase shown in their work is about 40 μm, which is smaller than ours. Such a difference may come from the formation process of the SF/PEO blend film, because we used more dilute solutions (both SF and PEO solutions are 1% (w/w)) than Kaplan *et al*. used (8% (w/w) SF solution and 5% PEO (w/w) solution). The slow drying process in our work may allow the phase separation to proceed further, leading to larger domains. To support this assumption, we prepared our SF/PEO blend film in a desiccator, in which the relative humidity was lower than 10%, leading to a faster drying process compared to the normal air dry. The FTIR image of such a SF/PEO blend shows the domain size of 30–40 μm (Fig. S1), which is obviously smaller than the ones in those air-dry films. This implies FTIR imaging can provide direct, quick, and visualized approach to observe the domain sizes in the blend films prepared under different conditions. In addition, the change of the blend composition also leads the variation of domain size. For instance, Kaplan *et al*. observed SF globules with the size of 100–200 μm in SF/PEO blend at 95/5 ratio.[8]

SF conformation in SF-rich and PEO-rich phases

FTIR imaging not only offers the possibility to observe the phase behaviour of SF/PEO blend but also to monitor structural information from each component in specific phase or position. Fig. 2a shows FTIR spectra of the SF-rich domain and PEO-rich matrix extracted from single pixels of the FTIR image shown in Fig. 1b. It shows the characteristic absorption of PEO (1113 cm^{-1}) obviously decreases from the PEO-rich phase to the SF-rich phase. In the amide I band, although it is observed in both the SF-rich and PEO-rich phases, the shape of the band differs significantly. The FTIR spectra extracted from the SF-rich domains have a peak maximum at 1660 cm^{-1}, indicating random coil and/or helical conformation is dominant in the SF-rich regions. However, it shows a strong absorption at 1630 cm^{-1} with a shoulder peak at 1700 cm^{-1} in the FTIR spectra extracted from PEO-rich matrix, which clearly demonstrates SF transits from random coil and/or helix into β-sheet in this region. From the PEO-rich phase to the SF-rich phase (direction of arrow), both the intensity and the peak

position change gradually but significantly, indicating both the content and the conformation of SF are different in these two phases.

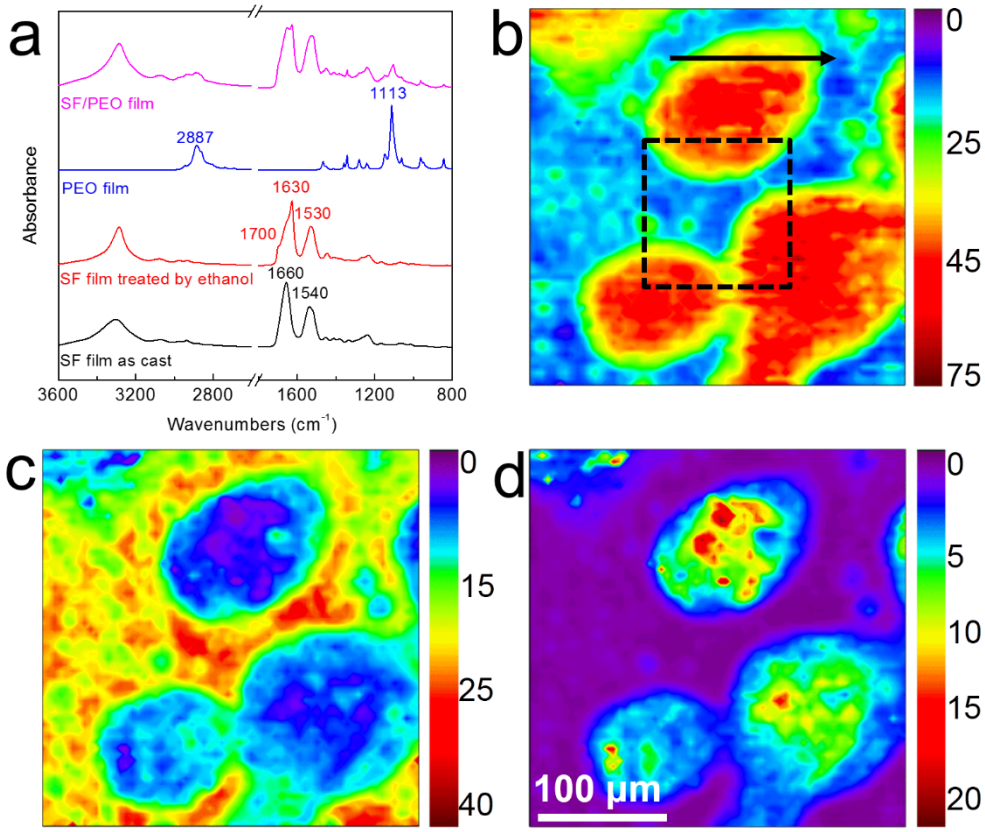

Fig. 1 FTIR spectra and FTIR images of SF/PEO blend. (a) FTIR spectra of SF film as cast, SF film treated with 70% ethanol solution, pristine PEO film, and SF/PEO blend film; (b) SF-specific FTIR image of SF/PEO blend; (c) PEO-specific image of SF/PEO blend; (d) A_{SF}/A_{PEO} image of SF/PEO blend. The scale bars in (b), (c), and (d) are the same.

In order to completely compare the conformation difference in each pixel of the FTIR map, we used *k*-mean cluster analysis with 2 clusters to image the normalized amide I band, and present the result in Fig. 2b. The profile of the cluster image is very similar to those FTIR images shown above (Fig. 1b-d), as would be expected. The mean amide I bands of each cluster (Fig. 2c for "island" and Fig. 2d for "sea" regions) are in close agreement with the extracted single pixel spectra (Fig. 2a). Then we tried to deconvolute the amide I bands in the FTIR image to compare the β-sheet content in different regions in SF/PEO blend. For convenience, we selected a small 25 × 25 pixel area to perform the deconvolution, and the selected area is marked by white dotted box in Fig. 2b. We used the same deconvolution method as described in our previous works,[27] and the typical deconvolution results can be inspected in Fig. 2c and 2d. We use three peaks to do the deconvolution because there are only three conformations, *i.e.*, random coil and/or helix (shortened to random coil in Fig. 2), β-sheet, and β-turn associated with β-sheet (shortened to β-turn in Fig. 2) can be found in SF samples if they were measured under well-controlled conditions — the trace of water in the sample and along the infrared light path in the spectrometer was totally removed by thorough nitrogen/dry air purge or vacuuming the infrared spectrometer. Details can be found in a series of our previous publications.[27,34-36] The β-sheet content image of the selected area is presented in Fig. 2e, and it is found that the SF-rich domains have very little β-sheet (<10%), but PEO-rich matrix has much more (20–30%). In addition, the shape of the boundary in Fig. 2e is very similar to those in Fig. 1d and 2b, which further confirms the significant difference in β-sheet structure in the SF-rich and PEO-rich phase of SF/PEO blend.

STXM imaging of SF/PEO blends

The results shown above in addition to those presented in our previous work[19] clearly demonstrate that FTIR imaging is a powerful tool for studying the phase behaviour and protein conformation in SF-based polymer blends. However, because of the diffraction limit, FTIR imaging technique is only suitable for those SF-based polymer blends whose phase size is larger than 4 μm. STXM imaging, whose resolution reaches 30 nm or better, is a good candidate for the investigation of the smaller phases.

Fig. 3a shows the NEXAFS spectra of pristine SF and PEO films. Both spectra display a step-increase in absorption (the carbon K-edge) near 290 eV and a weak carbon-carbon π* resonance near 284 eV. However, SF has an intense, sharp amide π* absorption peak at the photon energy of 288.25 eV,[24] while PEO shows a broader C-H Rydberg/σ* absorption peak at 289.05 eV.[42] Such a difference in the absorption spectra between SF and PEO is easily sufficient for the basis of observed chemical contrast in the STXM images presented in this work.

Fig. 3b and c present SF and PEO composition images (percentage by volume) of SF/PEO blend in an area of 10 × 10 μm.

They clearly show a pattern of SF-rich domains dispersed in a PEO-rich matrix similar to the FTIR images shown in Fig. 1. However, the size of SF-rich domains is about 2 μm, which is much smaller than those seen in the FTIR images. We also attribute this difference to the sample formation process, with the STXM sample produced from a much smaller drop of solution that dried more quickly to form a thinner, less evolved morphology compared to the 5 μm thick film prepared for FTIR imaging.

Fig. 3d shows a thickness image of the SF/PEO blend, which is a useful feature of STXM imaging that cannot be obtained from FTIR imaging. Note that the pattern in thickness in Fig. 3d is almost identical to the SF and PEO composition images shown in b and c. By comparing these images, we can see that the SF-rich domain is thicker than the PEO-rich matrix, as might be expected from the lower solubility of the SF in the water solvent than PEO. The cross-sectional trace presented in Fig. 3e (location shown in parts b and d) shows that the SF-rich domain is about 110 nm thick and contains 74±4% silk protein, while the PEO-rich matrix is only about 70 nm thick and has 38±6% silk protein. The trace also shows that the domain boundaries are quite sharp compared to the width of the domains.

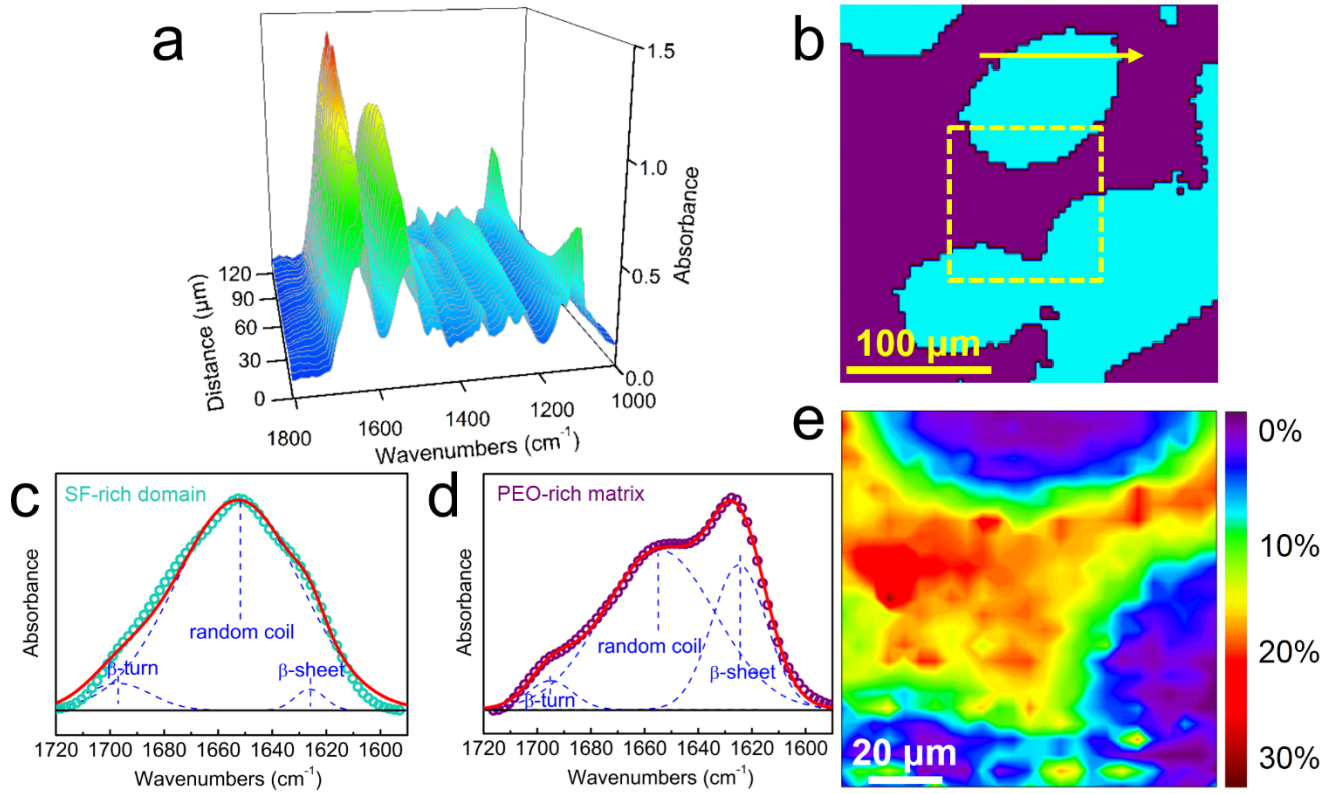

Fig. 2 Conformation difference of SF in SF-rich and PEO-rich phase. (a) FTIR spectra extracted from FTIR image as indicated in Fig. 1b along the direction of arrow (for convenience, the arrow at the same position is also shown in part b of this figure); (b) *k*-mean cluster analysis image of SF/PEO blend by using normalized amide I bands; (c) the mean amide I band of cyan area in (b) and the corresponding deconvolution results (circles, original spectrum; dashed curve, deconvoluted peaks; solid curve, simulated spectrum from summed peaks); (d) the mean amide I band of purple area in (b) and the corresponding deconvolution results (circles, original spectrum; dashed curve, deconvoluted peaks; solid curve, simulated spectrum from summed peaks); (e) β-sheet percentage map in the region marked by dashed box shown in (b).

Phase separation in SF/PEO blends

We know SF is composed of small hydrophilic and dominant hydrophobic blocks (GAGAGS repetitive motifs that are known to form anisotropic β-sheet-rich nanocrystals), with larger hydrophilic blocks at the chain ends. Thus, SF acts as a hydrophilic-hydrophobic-hydrophilic block copolymer, which is unstable and exist as colloidal state in aqueous systems due to the hydrophilic blocks forming a solubilizing shell around the hydrophobic blocks.[8] On the other hand, PEO readily dissolves in water and forms a stable aqueous solution. Thus, during the drying process of the SF/PEO blend solution, the concentration increases as water evaporates, driving SF micelles to aggregate into "globules" that grow with time until the SF loses mobility due to the lack of water. Therefore a fast drying process results in smaller SF-rich domains (about 2 μm, Fig. 3b–d) as we found in STXM imaging, while the thicker film prepared for FTIR imaging showed increased domain size (30–40 μm when dried in the desiccator, Fig. S1, and 80–100 μm for air dry, Fig. 1b–d) because it needed a much long time to dry, prolonging the mobility of the SF.

In addition to the water evaporation during the film formation process, the hydroscopicity of PEO also caused the loss of water from the micelles. The rapid loss of water "freezes" the conformation of SF in micelles, which is why we observed the random coil and/or helical conformation to dominate in the SF-rich phase (Fig. 2a). On the contrary, those SF molecules not involving the formation of micelles (dispersed in PEO) were plasticized by water absorbed in PEO, which then have the mobility to adjust their conformation to form β-sheet, as our results demonstrate with greater β-sheet conformation of the SF in the PEO-rich phase. Thus,

our findings from FTIR imaging is quite compatible with the hypothesis proposed by Kaplan *et al*. [8]

Although phase separation occurred during the formation of the SF/PEO blend films, it was shown that SF and PEO coexisted in both phases by both FTIR and STXM imaging. We know from the theory of polymer blends that both components normally coexist in different phases, but it is quite difficult to determine with the conventional methods (SEM, AFM, DSC, and DTMA). Here we demonstrate that both FTIR and STXM imaging can provide such information, though FTIR imaging may only give qualitative one, whereas STXM is able to provide quantitative results on the composition of the components in each phase. Moreover, it could be possible to use both FTIR and STXM imaging techniques to a same sample. The relatively thick FTIR sample can be ultrathin sectioned to meet the requirement for STXM imaging study.

As with many others techniques, both FTIR and STXM imaging have their own limitation. Normally, the basis of the imaging technique is the difference in the absorption of the characteristic peaks of the components. The amide bands (amide I, II, III, etc.) in FTIR and amide π* absorption in NEXAFS spectroscopy can be distinguishable from other polymer component in most cases, so it is why we claim these two methods are suitable for studying protein-based polymer blends. Though it may encounter difficulties when study protein/protein blends, we can use more advanced multivariate imaging approaches, such as principal component analysis[43] and cluster analysis[44] (already used in this work) to analyze those FTIR or STXM imaging data. These analytical methods are not like univariate imaging (also called "function group imaging", which just uses intensity or areas of a specific peak), but use a whole spectra (or an interesting region, such as fingerprint region) to analyze. Thus, we can distinguish the subtle differences in the spectra of different components, and widen the application area of this promising analytical method, the combination of FTIR and STXM imaging.

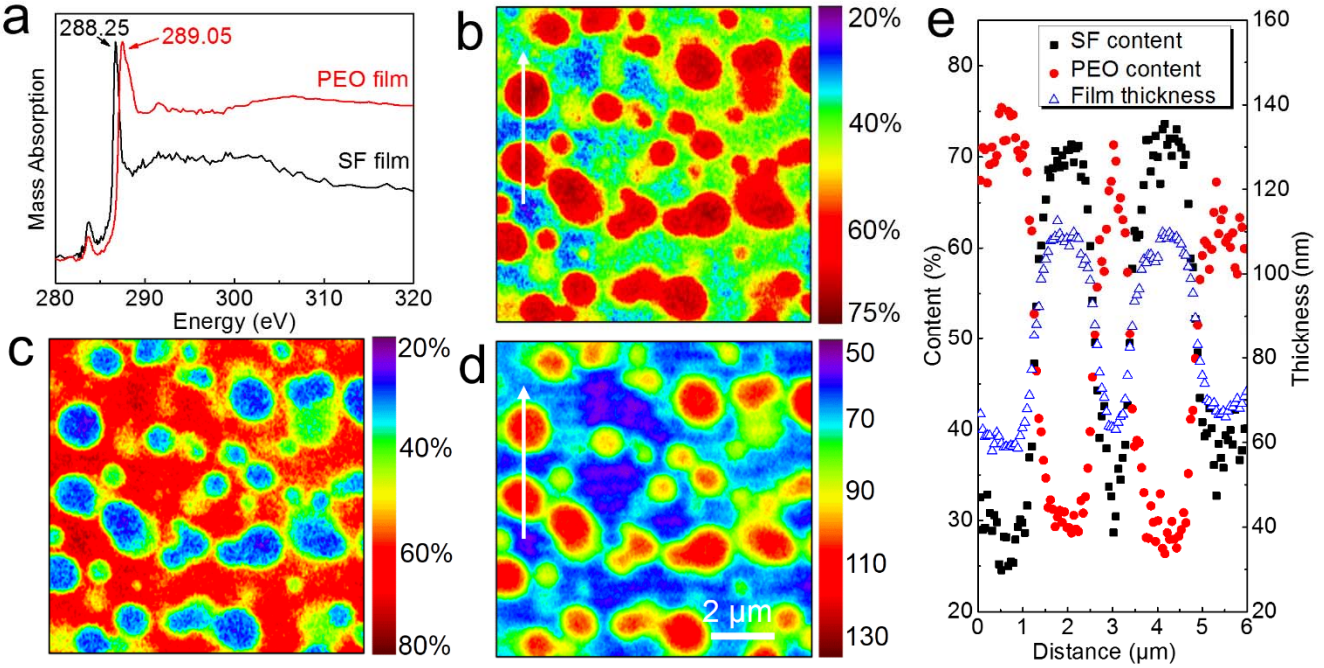

Fig. 3 (a) Near-edge X-ray absorption fine structure (NEXAFS) spectra of pristine SF and PEO film; (b) SF composition image of SF/PEO film; (c) PEO composition image of SF/PEO film; (d) STXM-derived thickness image of SF/PEO film; (e) cross-sectional composition traces (black squares, SF; red circles, PEO) and calculated thickness (blue hollow triangle) of SF/PEO film along the arrow in (b) or (d). The scale bars in (b), (c), and (d) are the same.

Conclusions

In this paper, we report the use of two chemical imaging techniques, FTIR imaging and STXM imaging to investigate the structure of SF/PEO blend films. We demonstrate that FTIR imaging is not only able to study the phase separation behaviour with the resolution of 4 μm, but also can analyze the molecular conformation in the specific regions of the blend. The FTIR images clearly show that there is a strong phase separation in the SF/PEO blend, in which 80–100 μm diameter SF-rich domains are dispersed in a PEO-rich matrix. SF exhibits random coil and/or helical conformation in the dispersed domains, but β-sheet conformation in the matrix. Such a conformation difference may provide a new strategy in the design of SF materials that make use of different structures in different regions. However, the limitation of the resolution of FTIR imaging prevents this technique from monitoring the phase separation in morphologies smaller than about 4 μm. To solve this issue, we introduce STXM imaging, which is not only able to provide high resolution images of the phase morphology, but also provides quantitative thickness and composition maps. We found the thickness and the SF content in SF-rich and PEO-rich phase were different, which were 100 nm and 70 nm, and 74±4% and 38±6%, respectively.

A combination of FTIR and STXM imaging offers the possibility to obtain both spectral and spatial information, thereby enabling a powerful visualization of samples. An experimental strategy integrating these techniques is very useful to fully understand the structure of polymer blends, especially the SF-based blends or other protein-based (for instance, collagen and soy

protein) blends, as it can provide detailed information of phase morphology, composition and thickness of each phase, as well as the protein conformation.

Acknowledgments

This work is supported by the National Natural Science Foundation of China (Nos. 10979022, 20974025, and 21034003). Shengjie Ling gratefully acknowledges the provision of a scholarship by the China Scholarship Council and Prof. Dr. Raffaele Mezzenga at ETH Zürich to support his experiments in Swiss Light Source, Paul Scherrer Institute. The authors also thank Dr. Jinrong Yao and Dr. Yuhong Yang at Fudan University for their valuable suggestions and discussions. The PolLux endstation is financed by the German Minister für Bildung und Forschung (BMBF) through contracts 05KS4WE1/6 and 05KS7WE1.

Notes and references

[a] *State Key Laboratory of Molecular Engineering of Polymers, Department of Macromolecular Science, Laboratory of Advanced Materials, Fudan University, Shanghai, 200433, People's Republic of China. Fax: 86 21 5163 0300; Tel: 86 21 6564 2866; E-mail: chenx@fudan.edu.cn*

[b] *National Synchrotron Radiation Laboratory, University of Science and Technology of China, Hefei, 230029, People's Republic of China*

[c] *Swiss Light Source, Paul Scherrer Institute, Villigen-PSI, CH-5232, Switzerland*

1 J. G. Hardy and T. R. Scheibel, *Prog. Polym. Sci.*, 2010, **35**, 1093-1115.
2 D. N. Rockwood, R. C. Preda, T. Yucel, X. Q. Wang, M. L. Lovett and D. L. Kaplan, *Nat. Protoc.*, 2011, **6**, 1612-1631.
3 D. L. Kaplan and C. Vepari, *Prog. Polym. Sci.*, 2007, **32**, 991-1007.
4 B. Kundu, R. Rajkhowa, S. C. Kundu and X. G. Wang, *Adv. Drug Deliv. Rev.*, 2013, **65**, 457-470.
5 E. Wenk, H. P. Merkle and L. Meinel, *J. Control. Release*, 2011, **150**, 128-141.
6 M. Tsukada, G. Freddi and J. S. Crighton, *J. Polym. Sci. Part B: Polym. Phys.*, 1994, **32**, 243-248.
7 I. C. Um and Y. H. Park, *Fibers Polym.*, 2007, **8**, 579-585.
8 H. J. Jin and D. L. Kaplan, *Nature*, 2003, **424**, 1057-1061.
9 H. J. Jin, J. Park, R. Valluzzi, P. Cebe and D. L. Kaplan, *Biomacromolecules*, 2004, **5**, 711-717.
10 B. D. Lawrence, F. Omenetto, K. Chui and D. L. Kaplan, *J. Mater. Sci.*, 2008, **43**, 6967-6985.
11 T. Tanaka, T. Tanigami and K. Yamaura, *Polym. Int.*, 1998, **45**, 175-184.
12 S. J. Park, K. Y. Lee, W. S. Ha and S. Y. Park, *J. Appl. Polym. Sci.*, 1999, **74**, 2571-2575.
13 J. Koenig, *Adv. Mater.*, 2002, **14**, 457-460.
14 R. Bhargava, S. Q. Wang and J. L. Koenig, *Adv. Polym. Sci.*, 2003, **163**, 137-191.
15 C. Vogel, E. Wessel and H. W. Siesler, *Biomacromolecules* 2008, **9**, 523-527.
16 C. Vogel, E. Wessel and H. W. Siesler, *Macromolecules*, 2008, **41**, 2975-2977.
17 B. A. Miller-Chou and J. L. Koenig, *Macromolecules*, 2003, **36**, 4851-4861.
18 C. Vogel, E. Wessel and Siesler, H. W. *Appl. Spectrosc.*, 2008, **62**, 599-603.
19 S. J. Ling, Z. M. Qi, D. P. Knight, Z. Z. Shao and X. Chen, *Polym. Chem.*, 2013, **4**, 5401-5406.
20 M. J. Nasse, M. J. Walsh, E. C. Mattson, R. Reininger, A. Kajdacsy-Balla, V. Macias, R. Bhargava and C. J. Hirschmugl, *Nat. Methods*, 2011, **8**, 413-U58.
21 C. R. McNeill, B. Watts, L. Thomsen, W. J. Belcher, N. C. Greenham and P. C. Dastoor, *Nano Lett.*, 2006, **6**, 1202-1206.
22 B. Watts, and C. R. McNeill, *Macromol. Rapid Commun.*, 2010, **31**, 1706-1712.
23 B. Watts, T. Schuettfort and C. R. McNeill, *Adv. Funct. Mater.*, 2011, **21**, 1122-1131.
24 D. H. Cruz, M. E. Rousseau, M. M. West, M. Pezolet and A. P. Hitchcock, *Biomacromolecules*, 2006, **7**, 836-843.
25 M. E. Rousseau, D. H. Cruz, M. M. West, A. P. Hitchcock and M. Pezolet, *J. Am. Chem. Soc.*, 2007, **129**, 3897-3905.
26 X. Q. Wang, T. Yucel, Q. Lu, X. Hu and Kaplan, D. L. *Biomaterials*, 2010, **31**, 1025-1035.
27 S. J. Ling, Z. M. Qi, D. P. Knight, Z. Z. Shao and X. Chen, *Biomacromolecules*, 2011, **12**, 3344-3349.
28 U. Flechsig, C. Quitmann, J. Raabe, M. Booge, R. Fink and H. Ade, *AIP Conf. Proc.*, 2007, **879**, 505-508.
29 J. Raabe, G. Tzvetkov, U. Flechsig, M. Boge, A. Jaggi, B. Sarafimov, M. G. C. Vernooij, T. Huthwelker, H. Ade, D. Kilcoyne, T. Tyliszczak, R. H. Fink and C. Quitmann, *Rev. Sci. Instrum.*, 2008, **79**, 113704.
30 U. Frommherz, J. Raabe, B. Watts, R. Stefani and U. Ellenberger, *AIP Conf. Proc.*, 2010, **1234**, 429-432.
31 B. Watts, C. R. McNeill and J. Raabe, *Synth. Met.*, 2012, **161**, 2516-2520.
32 http://unicorn.mcmaster.ca/aXis2000.html
33 W. H. Moore and S. Krimm, *Biopolymers*, 1976, **15**, 2465-2483.
34 X. Chen, Z. Z. Shao, N. S. Marinkovic, L. M. Miller, P. Zhou and M. R. Chance, *Biophys. Chem.*, 2001, **89**, 25-34.
35 X. Chen, Z. Z. Shao, D. P. Knight and F. Vollrath, *Proteins*, 2007, **68**, 223-231.
36 X. Chen, D. P. Knight and Z. Z. Shao, *Soft Matter*, 2009, **5**, 2777-2781.
37 Y. Zheng, M. L. Bruening and G. L. Baker, *Macromolecules*, 2007, **40**, 8212-8219.
38 Y. Geng, G. L. Wang, Y. H. Cong, L. G. Bai, L. B. Li and C. L. Yang, *J. Polym. Sci. Part B: Polym. Phys.*, 2010, **48**, 106-112.
39 T. Yoshihara, S. Murahashi and H. Tadokoro, *J. Chem. Phys.*, 1964, **41**, 2902-2911.
40 C. X. Liang and K. Hirabayashi, *J. Appl. Polym. Sci.*, 1992, **45**, 1937-1943.
41 X. Chen, W. J. Li and T. Y. Yu, *J. Polym. Sci. Part B: Polym. Phys.*, 1997, **35**, 2293-2296.
42 O. Dhez, H. Ade and S. G. Urquhart, *J. Electron Spectrosc. Relat. Phenom.*, 2003, **128**, 85-96.
43 F. Bonnier and H. J. Byrne, *Analyst*, 2012, **137**, 322-332.
44 P. Lasch, W. Haensch, D. Naumann and M. Diem, *Biochim. Biophys. Acta-Mol. Basis Dis.*, 2004, **1688**, 176-186.